AMERICAN
METEOROLOGICAL
SOCIETY

Journal of Physical Oceanography

EARLY ONLINE RELEASE

The DOI for this manuscript is doi: 10.1175/JPO-D-17-0124.1

On the relationship between the energy dissipation rate of surface breaking waves and oceanic whitecap coverage.

Adrian H. Callaghan[1,2,*]

[1] Department of Civil and Environmental Engineering, Imperial College, London, UK.

[2] Formerly at Scripps Institution of Oceanography, University of California, San Diego, La Jolla, California, USA.

[*] Email address for correspondence: a.callaghan@ic.ac.uk

Abstract

Wave breaking is the most important mechanism that leads to the dissipation of oceanic surface wave energy. A relationship between the energy dissipation rate associated with breaking wave whitecaps (S_{wcap}) and the area of whitecap foam per unit area ocean surface (W) is expected, but there is a lack of consensus on what form this relationship should take. Here, mathematical representations of whitecap coverage (W), and growth phase whitecap coverage (W_{growth}) are derived, and an energy-balance approach is used to formulate W and W_{growth} in terms of S_{wcap}. Both W and W_{growth} are found to be linearly proportional to S_{wcap}, but also inversely proportional to the bubble plume penetration depth during active breaking. Since this depth can vary for breaking waves of different scales and slopes, there is likely no unique relationship between S_{wcap} and either W or W_{growth} as bubble plume penetration depth must also be specified. Whitecap observations from the North Atlantic are used to estimate bubble plume penetration depth as a function of wind speed, and then used with W measurements to compute S_{wcap}. An estimate of the relative magnitude of S_{wcap} to the rate of energy input from the wind to the waves, S_{in}, is made. Above wind speeds of about 12 m/s, S_{in} is largely balanced by S_{wcap}. At lower wind speeds the ratio S_{wcap}/S_{in} quickly drops below unity with decreasing wind speed. It is proposed that sea state driven variability in both S_{wcap}/S_{in} and bubble plume penetration depth are significant causes of variation in whitecap coverage datasets and parameterizations.

Introduction

Wind-driven breaking waves are ubiquitous throughout the global oceans and seas, and occur in a variety of forms in all but the calmest of sea states. Wave breaking limits the height of individual waves, generates turbulence that helps mix the upper ocean, entrains air which drives bubble-mediated ocean-atmosphere exchange processes, and generates extreme surface flows (Melville 1996). Predicting and measuring the occurrence, severity, and scale of breaking waves remain active areas of research with important consequences for operational wave modelling, air-sea interaction studies, climate modelling, and setting engineering design criteria.

In an equilibrium sea state, the rate of wind energy input to the upper ocean is balanced by the rate of energy dissipation associated with wave breaking, wind-driven turbulence, Langmuir turbulence and swell waves (e.g. Oakey and Elliott 1982; Belcher et al. 2012; Ardhuin et al. 2009; Banner and Morison, 2010, Thomson et al. 2013, 2016). Of these, wave breaking is commonly assumed to be the dominant dissipative process (Cavaleri et al. 2007), and the other processes have been previously described collectively as background dissipative processes (e.g., Thomson et al., 2016). These background dissipative processes are important in their own right, but will not be considered individually in detail here because they are not directly related to wave breaking.

When waves break, wave energy is transformed into turbulent kinetic energy, some of which is converted to heat by viscous forces (Thorpe 2005). When the breaking process is sufficiently energetic, enough air is entrained such that the associated broadband scattering of light gives rise to a distinctive visible whitecap (Monahan 1971). Microscale breaking waves also dissipate wave energy but do not form distinctive whitecaps (Banner and Phillips 1974),

and infra-red techniques are commonly used to image these breakers (Jessup et al. 1997). There is acoustic evidence that small oceanic breaking waves occurring at wind speeds as low as 1.5 m/s may entrain small amounts of air, but do not form distinctive whitecaps (Updegraff and Anderson 1991). These may be related to microscale breaking waves which according to Banner and Phillips (1974) can entrain some air, described as "*very little air*", but are often classified as non-air entraining. Even if they entrain some air, per unit length breaking crest, air entrainment in microscale breakers is certainly much less than in whitecaps, but their occurrence may be more widespread (Banner and Phillips 1974).

Air-entrainment by breaking waves helps drive air-sea exchange processes that alter the composition of the ocean and atmosphere through bubble-mediated exchange of climatically relevant gases such as CO_2 (Woolf 2005). Furthermore, primary marine sea spray aerosol (SSA) particles, which are important pre-cursors to cloud condensation nuclei, are generated by bursting bubbles at the ocean surface formed primarily by whitecaps (deLeeuw et al. 2011). Gas exchange and SSA particle production fundamentally affect the earth's climate: the former acts to buffer the rise in atmospheric CO_2 concentrations due to the burning of fossil fuels, and the latter influences the earth's radiation budget through cloud formation and scattering of solar radiation.

The presence of whitecap foam on the sea surface is an indicator of the occurrence, or recent occurrence, of breaking wave whitecaps. The fractional coverage of the ocean surface with whitecap foam is denoted W, and estimates of W are often used to force parameterizations of SSA production flux and rates of bubble-mediated gas exchange (e.g. Monahan et al., 1986; Fairall et al. 2011; Grythe et al. 2014; Goddijn-Murphy et al. 2016; Bell et al. 2017). Furthermore, the variation of W is of interest in its own right because whitecap foam (i)

increases the sea surface albedo and emissivity, (ii) affects the passive remote sensing of the ocean surface and (iii) complicates the remote measurement of the ocean wind vector and ocean color using satellite-based instrumentation (Gordon 1997; Frouin et al. 2001; Quilfen et al. 2007). It has been also proposed that a comparison between W measurements and estimates derived from models could be used to provide a further constraint on the performance of the dissipation term in spectral wave models (Cavaleri et al. 2007; Banner and Morison 2010; Leckler et al. 2013).

It is evident that improved models and parameterizations of W have the potential to benefit a wide range of areas of study. The variation in W has, more often than not, been parameterized only as a function of the mean horizontal wind speed at a height of 10 m above the sea surface, u_{10} (Anguelova and Webster, 2006). However since the occurrence, scale and intensity of wave breaking is not uniquely linked to wind speed, a large variation in W values is possible for a given u_{10}. It is therefore desirable to seek models and parameterizations for W that are explicitly dependent on wave field properties, as well as incorporating wind speed information. Indeed, Brumer et al. (2017) showed that variation in W measured in multiple field campaigns across a wide range of wind speeds was well-explained using a combination of both significant wave height and u_{10}.

Since breaking waves dissipate wave energy, perhaps the most fundamental variable that could be used to model variability in W is the energy dissipation rate associated with breaking wave whitecaps (Kraan et al. 1996; Anguelova and Hwang 2016). A connection between W and whitecap energy dissipation rate is intuitively expected and many previous studies have assumed a linear relationship between the two quantities (e.g., Ross and Cardone 1974; Wu 1979; Hwang and Sletten 2008; Goddijn-Murphy et al. 2011; Scanlon et al. 2016).

Monahan (1971), however, suggested that the rate of whitecap area formation, as opposed to W, is more closely linked to the breaking wave energy dissipation rate, whereas others have suggested that Stage A whitecap coverage (W_A) is more appropriate (Kraan et al. 1996; Anguelova and Hwang 2016; Scanlon et al. 2016). Stage A whitecaps were described by Monahan and Woolf (1988) as "*surface manifestations of plunging aerated plumes*", and W_A is understood to represent foam coverage by actively breaking waves (Kleiss and Melville, 2011; Anguelova and Hwang, 2016).

The exact nature of the relationship between breaking wave energy dissipation rate and either W or W_A has not yet been firmly established. A linear relationship implies that the dissipation rate of wave energy per unit area whitecap is constant. In support of this, Scanlon et al. (2016) reported a linear relationship between breaking wave energy dissipation rate from a spectral wave model and field measurements of both W and W_A. Schwendeman and Thomson (2015) also observed a largely linear dependence between measured turbulent kinetic energy dissipation rate in the upper 60 cm of the water column and co-incident measurements of W. Hwang and Sletten (2008) and Goddijn-Murphy et al. (2011) have also had reasonable success in fitting a linear model of wave energy dissipation rate to a collection of W datasets.

Notwithstanding these results, however, there is sufficient variability across studies to prompt a detailed evaluation of this linear assumption, as studies often exhibit an order of magnitude or more variability in their datasets (e.g. Hwang and Sletten 2008; Schwendeman and Thomson 2015; Scanlon et al. 2016). For example, using field measurements Hanson and Phillips (1999) suggested a weakly non-linear relationship between W and total wave energy dissipation rate, and Schwendeman and Thomson (2015) found little statistical difference

between linear and quasi-quadratic dependencies. Furthermore, for a given wind energy input rate at the ocean surface, the relative degree of energy dissipation due to whitecapping, microscale breaking and background processes is sea state dependent (Sutherland and Melville 2013, 2015; Banner and Morison 2018). In other words, the fraction of the total wave energy dissipated by whitecaps is not fixed in an equilibrium sea state. Moreover, because energy dissipation by whitecaps occurs within the two-phase flow beneath the surface whitecap, it does not automatically hold that the sub-surface three-dimensional energy dissipation rate should scale linearly with two-dimensional surface W or W_A. This is especially true when the possibility of variable bubble plume penetration depth is considered, something which is possible for breaking waves with different steepness. Additionally, whitecap foam can be stabilized by surfactants present in the upper ocean, further complicating any relationship between W and models of wave energy dissipation rate, as was discussed by Ross and Cardone (1974). This is less of a concern when considering W_A measurements, as previously recognized (Kraan et al. 1996; Anguelova and Hwang 2016).

To better understand the relationship between whitecap coverage and the breaking wave energy dissipation rate, a mathematical formulation is needed that explicitly accounts for air entrainment, bubble plume degassing, and surfactant-driven foam stabilization. The degree of air entrainment is closely linked to the total, and rate of, breaking wave energy dissipation (Duncan, 1981; Lamarre and Melville, 1991; Blenkinsopp and Chaplin 2007; Callaghan et al. 2016; Deane et al. 2016), and both bubble plume degassing, and foam stabilization influence whitecap lifetime (Callaghan et al., 2013, 2017). In addition, the fraction of the wind energy input flux to the upper ocean that is dissipated by whitecaps and background processes including microscale breaking waves, should be explicitly accounted for.

The goal of this study therefore, is to develop a physically-based model of whitecap coverage (i) that is dependent on balancing the wind energy flux at the ocean surface with the overall energy dissipation rate within the upper ocean, (ii) that highlights the role of specific physical parameters such as bubble plume penetration depth that affect the evolving foam properties of individual whitecaps, and (iii) that can be used with existing datasets of whitecap coverage to infer the dissipation rate associated with breaking wave whitecaps. The approach taken builds upon recent results from laboratory and field experiments that have highlighted the relative importance of breaking wave whitecaps and background dissipative processes. While the effects of surfactant-driven foam stabilization on whitecap coverage are also explicitly addressed in the model formulation, surfactant effects are assumed to be small when the model is evaluated in subsequent sections due to insufficient data.

The paper proceeds as follows. A mathematical representation of whitecap coverage is presented that explicitly incorporates a whitecap growth phase driven by air entrainment, and a whitecap decay phase driven by bubble plume degassing and foam stabilization by surfactants. The laboratory results of Callaghan et al. (2016) are used to link total breaking wave energy dissipation with specific whitecap foam properties, leading to a model of whitecap coverage based on the energy dissipation rate associated with whitecaps. The field data of Scanlon and Ward (2016) are used with the model to parameterise the average bubble plume penetration depth associated with whitecaps as a function of wind speed. This is then combined with whitecap coverage observations of Callaghan et al. (2008) to estimate the rate of energy dissipated by whitecaps. The results are then used to infer the fraction of the wind energy input rate to the wave field that is dissipated by breaking wave whitecaps, with results compared to similar estimates from Banner and Morison (2018).

2. A Mathematical Representation of Whitecap Coverage

A glossary of all variables is given in Table A1 in appendix A. The measured temporal evolution of foam area, $A(t)$, of an oceanic whitecap is depicted in figure 1. The accompanying annotations follow the conceptual model of foam evolution presented in figure 2b in Callaghan et al. (2017), hereafter referred to as CDS17. The peak in foam area, A_o, occurs at a time t_{Ao}, and is used to delineate the whitecap growth and decay phases. It is understood that t_{Ao} represents the point at which whitecap area growth and decay processes are in equilibrium: for times $t < t_{Ao}$ during the whitecap growth phase air entrainment is expected to dominate, while during the decay phase ($t > t_{Ao}$) air loss through bubble degassing dominates. When present, the stabilizing effect of surfactants also influence foam decay, and this becomes important at the divergence timescale, $t = \tau_{div}$. This timescale marks the point at which measured foam area evolution $A(t)$ departs from the expected foam area growth and decay in the absence of surfactants, which is denoted $A_{GD}(t)$. A method to determine $A_{GD}(t)$ from $A(t)$ is given in CDS17, and their difference gives a measure of any surfactant effect which is quantified by the stabilization factor, Θ, defined in CDS17. For reference, $\Theta = 1.7$ for the whitecap in figure 1, which means surfactant-driven foam stabilization contributed an additional 70% of $A_{GD}(t)$ to the measured $A(t)$.

Wave breaking, air entrainment and foam evolution are extremely complicated processes, and the growth-decay decomposition presented here is a necessarily simplified representation of these processes. Nevertheless, it is a useful construct that can be applied to individual whitecaps as measured with digital image analysis techniques. It provides the basis for formulating a mathematical representation of W and W_{growth} in terms of breaking wave energy dissipation rate.

Assuming that foam patches from individual breaking waves do not overlap, whitecap coverage may be defined as the sum of the area-time-integral of each of M whitecaps following:

$$W = \frac{\sum_{i=1}^{M} \int_0^{\infty} A_i(t)dt}{A_{obs}T_{obs}}, \quad (1)$$

where A_{obs} is an observational area, and T_{obs} is an observational time period. There may be a difference between W and the measured whitecap coverage, W_{meas}, that is a function of some measurement efficiency, Γ, such that $W_{meas} = \Gamma W$. The value of Γ is expected to lie between 0 and 1, and to be dependent on properties of the imaging system, as well as variables related to the sun zenith and azimuthal angles, and the transmission of light through the atmosphere. For example, the value of Γ at night-time would be practically 0. It is beyond the scope of the current paper to critically assess Γ, but how variations in Γ affect W_{meas} should be the focus of future work. For the remainder of this work Γ is set to 1 and $W_{meas} = W$.

The whitecap area-time-integral in equation (1) can be separated into growth and decay contributions defined, respectively, as

$$\chi_{growth} = \int_0^{t_{Ao}} A_i(t)dt, \quad (2a)$$

and

$$\chi_{decay} = \int_{t_{Ao}}^{\infty} A_i(t)dt. \quad (2b)$$

In turn, W is written as the sum of growth and decay area-time-integrals associated with M individual whitecaps:

$$W = \frac{\sum_{i=1}^{M} \chi_{growth,i} + \chi_{decay,i}}{A_{obs}T_{obs}}. \quad (3)$$

The total area-time-integral depends on the horizontal extent of the surface whitecap, the bubble plume penetration depth during active breaking which influences the subsequent degassing time of the bubble plume, and the lifetime of foam at the water surface which can

be further modified by variations in water chemistry. Laboratory experiments have shown that (i) more energetic breaking waves entrain more air and produce larger two phase flows, (ii) deeper bubble plumes take longer to degas thus prolonging the surface whitecap expression, and (iii) surfactants increase foam lifetime at the water surface (Duncan 1981; Lamarre and Melville 1991; Blenkinsopp and Chaplin 2007; Deane et al. 2016; Callaghan et al. 2013, 2016, 2017). These physical and chemical processes affect the whitecap growth and decay phases differently, and should be explicitly accounted for.

The total energy dissipated by a breaking wave has been found experimentally to be proportional to the product of χ_{growth} and a measure of the bubble plume depth (Callaghan et al. 2016; hereafter referred to as CDS16), and deeper bubble plumes lead to larger values of χ_{decay}. Surfactant effects have been shown in CDS17 to primarily affect the latter stages of foam decay for 2-D unforced laboratory breaking waves, with minimal impact on χ_{growth}, and it is assumed that A_o, τ_{growth} and t_{Ao} are not adversely affected by surfactant effects.

In a model of W, it is desirable to explicitly account for the bubble plume degassing and surfactant-influenced regimes of foam decay in χ_{decay}, by writing it as the sum of a degassing term (χ_{degas}), and a foam stabilization term (χ_{stab}) . In the absence of the stabilizing effects of surfactants, the degassing of the bubble plume controls the surface whitecap area decay such that $\chi_{stab} = 0$, and $\chi_{decay} = \chi_{degas}$. The degassing area-time-integral χ_{degas} is written as:

$$\chi_{degas} = \int_{t_{Ao}}^{\infty} A_{GD}(t)dt, \qquad (4)$$

where $A_{GD}(t)$ is the foam area evolution in the absence of surfactants. When surfactant effects are important, χ_{decay} is a function of both plume degassing and surfactant-driven

foam stabilization. The contribution of foam stabilization to χ_{decay} can be evaluated using the integrated difference between $A(t)$ and $A_{GD}(t)$, and χ_{stab} is defined as:

$$\chi_{stab} = \int_{t_{Ao}}^{\infty} A(t) - A_{GD}(t)dt. \quad (5)$$

The area-time-integrals defined thus far may be written in terms of the product of A_o and a suitably defined timescale. The whitecap growth and degassing timescales are, respectively, $\tau_{growth} = A_o^{-1} \int_0^{t_{Ao}} A(t)dt$ and $\tau_{degas} = A_o^{-1} \int_{t_{Ao}}^{\infty} A(t)dt$. It then follows that a stabilization timescale, τ_{stab}, can be defined as $\tau_{stab} = \tau_{decay} - \tau_{degas}$.

The whitecap growth phase, bubble plume degassing phase and surfactant-driven foam stabilization phase can be combined to give the following representation of whitecap coverage:

$$W = \frac{\sum_{i=1}^{M} \chi_{growth,i} + \chi_{degas,i} + \chi_{stab,i}}{A_{obs}T_{obs}}. \quad (6)$$

Finally, W can be written as the sum of a growth term and a decay term that is dependent on bubble plume degassing and surfactant-driven foam stabilization, resulting in

$$W = W_{growth} + W_{degas} + W_{stab}, \quad (7)$$

where the following definitions have been adopted:

$$W_{growth} = (A_{obs}T_{obs})^{-1} \sum_{i=1}^{M} \chi_{growth,i}, \quad (8a)$$

$$W_{degas} = (A_{obs}T_{obs})^{-1} \sum_{i=1}^{M} \chi_{degas,i}, \quad (8b)$$

$$W_{stab} = (A_{obs}T_{obs})^{-1} \sum_{i=1}^{M} \chi_{stab,i}. \quad (8c)$$

Equation (7) explicitly recognizes the contributions of air entrainment, air loss and surfactant-driven foam stabilization to whitecap coverage.

3. Relating W to Rates of Breaking Wave Energy Dissipation and Wind Energy Input

In an equilibrium sea state, the input of wind energy to the upper ocean and wave field is continuously dissipated by a combination of breaking wave whitecaps, microscale breaking waves and other background dissipative processes. Therefore, W should first be described in terms of energy dissipation rate by whitecaps only (S_{wcap} - W m^{-2}), and then related to the wind energy input rate (S_{in} - W m^{-2}) by accounting for the contributions from microscale breaking waves (S_{μ} - W m^{-2}) and the other background dissipative processes (S_{bg} - W m^{-2}), as mentioned previously.

3.1 Relating W to Whitecap Energy Dissipation Rate, S_{wcap}

The laboratory work of CDS16 found a linear relationship between total wave energy dissipation ΔE_T (kg m^2 s^{-2}), and the breaking wave two-phase flow volume integrated in time during the whitecap growth phase, also known as the plume volume-time-integral. These results reinforce similar laboratory and numerical results of others (e.g., Duncan (1981), Lamarre and Melville (1991), Blenkinsopp and Chaplin (2007), Deane et al. (2016), Deike et al. (2016)).

Specifically, CDS16 found the following relationship

$$\Delta E_T = \Omega \rho A_o \hat{z}_p \tau_{growth}, \tag{9}$$

where Ω is a turbulence strength parameter with units W kg^{-1}, ρ is water density and $\hat{z}_p$ is a whitecap area-weighted bubble plume penetration depth. The term $A_o \hat{z}_p \tau_{growth}$ is the volume-time-integral of the two-phase flow during the whitecap growth phase. The terms A_o and τ_{growth} can be measured with above-water digital imaging techniques for individual whitecaps, and CDS16 found that $\hat{z}_p$ could be parameterized in terms of τ_{degas}. In other words, CDS16 showed how above-water 2-D images of evolving whitecap foam can be used

to estimate ΔE_T for individual whitecaps. In cases where surfactant effects influence foam evolution, this complicating signal must be removed before estimating $\hat{z}_p$ from foam decay time, as outlined in CDS17.

The turbulence strength parameter in equation (9) reflects a space and time averaged dissipation rate of turbulent kinetic energy (ϵ) within the liquid phase of the actively breaking crest. It is dependent on the air fraction within the breaking wave whitecap as well as the magnitude of ϵ. The value of Ω was determined in the laboratory experiments of CDS16 as the slope of the relationship between measured energy loss (ΔE_T) and the volume-time-integral for a set of 20 breaking waves and then compared to measurements of Duncan (1981), Lamarre and Melville (1991) and Blenkinsopp and Chaplin (2007). It is taken here to be constant at Ω = 0.88 W kg^{-1}, although a narrow distribution around this value may be expected (see figure S4 in CDS16).

The use of a constant value of Ω is consistent with the idea that the space and time-averaged dissipation rate of turbulent kinetic energy within breaking waves that exceed a minimum scale saturates, and that the total energy dissipated in wave breaking and the resulting two-phase flow volume are proportional (Deane et al., 2016). Furthermore, the acoustic signature of a breaking wave is dependent on the number and size of bubbles created in the associated two-phase flow, and can yield information about the dissipation rate of turbulent kinetic energy within a breaking wave. The similarity in the acoustic signature of breaking waves in tropical cyclones at wind speeds up to 50 m s^{-1} (Zhao et al., 2014) and a laboratory study (Deane and Stokes, 2002) prompted Zhao et al. to speculate that the levels of turbulence in both datasets were similar despite the obvious discrepancy in forcing conditions and scale.

The appeal of the volume-time-integral model described by equation (9) is that it provides a convenient way to estimate the total energy loss due to breaking from easily-measureable properties of the breaking wave two-phase flow. It does not explicitly partition the energy dissipated by different processes. For detailed information on the partitioning of breaking wave energy losses due to fluid turbulence and bubble plume potential energy, the reader is referred to the modelling studies of Derakhti and Kirby (2014, 2016) and the laboratory study of Na et al. (2016).

By using equation (9) for a single whitecap, the total energy dissipated by a set of M whitecaps is given as:

$$\sum_{i=1}^{M} \Delta E_{T,i} = \Omega\rho \sum_{i=1}^{M} A_{o,i}\tau_{growth,i}\hat{z}_{p,i}. \qquad (10)$$

Values of $A_{o,i}$ and τ_{growth} have been reported in the literature (*e.g.*, Bondur and Sharkov 1982; Sharkov 2007; Callaghan et al. 2012; Callaghan 2013), but much less is known about the distribution of oceanic bubble plume penetration depths for actively breaking waves. Here, a whitecap growth-weighted mean bubble plume penetration depth, $\hat{z}_p^*$, is defined as

$$\hat{z}_p^* = \sum_{i=1}^{M} A_{o,i}\tau_{growth,i}\hat{z}_{p,i} \Big/ \sum_{i=1}^{M} A_{o,i}\tau_{growth,i}. \qquad (11a)$$

$\hat{z}_p^*$ is by definition constant for any given set of whitecaps, but can vary between different sets of whitecaps. By adopting the power law relationship between τ_{degas} and $\hat{z}_p$ reported in CDS16 (see their equation (13)), $\hat{z}_p^*$ can also be written entirely in terms of whitecap foam variables,

$$\hat{z}_p^* = \sum_{i=1}^{M} A_{o,i}\tau_{growth,i}\left[0.07 \times \left({\tau_{degas,i}}^{0.74}\right)\right] \Big/ \sum_{i=1}^{M} A_{o,i}\tau_{growth,i}. \qquad (11b)$$

The average loss of wave energy per unit sea surface area per unit time driven by whitecaps (S_{wcap}) is now written as:

$$S_{wcap} = \frac{\Omega \rho \hat{z}_p^* \sum_{i=1}^{M} A_{o,i} \tau_{growth,i}}{A_{obs} T_{obs}}. \quad (12)$$

Equation (12) can be rearranged to give the following relationship:

$$W_{growth} = \frac{S_{wcap}}{\Omega \rho \hat{z}_p^*}. \quad (13)$$

Equation (13) shows that W_{growth} is expected to be linearly proportional to S_{wcap} but also inversely proportional to $\hat{z}_p^*$. Consequently, W_{growth} is not uniquely related to S_{wcap}, or in other words, for a given value of S_{wcap}, a variety of W_{growth} values is possible depending on variations in bubble plume penetration depth. Under the assumption of constant Ω , equation (13) shows that $\hat{z}_p^*$ can be interpreted as a measure of the energy dissipation rate per unit whitecap area during the whitecap growth phase. Breaking waves of differing scales and slopes generated in the laboratory produce a range of plume penetration depths, and a wide range of breaking wave scales and sea states are found in the ocean. It therefore seems likely that $\hat{z}_p^*$ also varies in the field.

Using equation (7), equation (13) can be written to explicitly relate S_{wcap} to W to give

$$W = \frac{S_{wcap}}{\Omega \rho \hat{z}_p^*}(1 + \delta), \quad (14)$$

where the term δ represents the ratio of the sum of W_{degas} and W_{stab} to W_{growth}, and is defined as

$$\delta = \frac{W_{degas} + W_{stab}}{W_{growth}} = \frac{\sum_{i=1}^{M} \chi_{degas,i} + \chi_{stab,i}}{\sum_{i=1}^{M} \chi_{growth,i}}. \quad (15)$$

To exclude surfactant effects δ can be modified by setting W_{stab} to zero to give

$$\delta^* = \frac{W_{degas}}{W_{growth}} = \frac{\sum_{i=1}^{M} \chi_{degas,i}}{\sum_{i=1}^{M} \chi_{growth,i}}. \quad (16)$$

Replacing δ with δ^* in equation (14) gives

$$W = \frac{S_{wcap}}{\Omega \rho \hat{z}_p^*}(1 + \delta^*), \quad (17)$$

which is the value of W expected in the absence of measureable surfactant effects. Similarly to W_{growth}, W is dependent on $\hat{z}_p^*$, but is also dependent on δ or δ^*. A comprehensive physical interpretation of equation (13) and equation (17) is given in section 4.

3.2. Relating W to Wind Energy Input Rate, S_{in}

In equilibrium conditions, the rate of energy input to the upper ocean, S_{in}, is balanced by the rate of energy loss due to (i) breaking wave whitecaps (S_{wcap}), (ii) microscale breaking waves (S_μ), and (iii) background dissipative processes (S_{bg}). This provides the following energy balance equation:

$$S_{in} = S_{wcap} + S_\mu + S_{bg}. \tag{18}$$

where the sum of the terms on the right hand side quantify the total wave energy dissipation rate, S_{diss}. The terms S_{wcap} and S_μ represent the total energy dissipation rate due to breaking waves (S_{brk}) such that $S_{brk} = S_{wcap} + S_\mu$. Alternatively, the sum of S_μ and S_{bg} may be used to quantify energy dissipation rate due to processes other than whitecapping, S_{other}, such that $S_{other} = S_\mu + S_{bg}$.

The measurements of Sutherland and Melville (2015) show that the relative values of S_{wcap} and S_μ are not fixed but are sea state dependent, changing as a function of wave age. This can be encapsulated by writing $S_\mu = \Phi S_{brk}$ where Φ represents the fraction of S_{brk} due to microscale breaking waves. The value of Φ is variable lying between 0 and 1. In low wind and swell-dominated wave conditions, Sutherland and Melville (2015) found S_{brk} to be dominated by S_μ, and the value of Φ was found to be as large as 0.9. In contrast, during conditions of strong winds and locally-driven wind seas, Φ was closer to 0.2 and S_{wcap} dominated the S_{brk} term. In a further re-analysis of the Sutherland and Melville (2015)

dataset, Banner and Morison (2018) suggest that both S_μ and S_{bg} may indeed become negligible at wind speeds in excess of about 12 m/s. In other words, in these strongly forced equilibrium conditions, $S_{wcap} \approx S_{diss} = S_{in}$. In summary, both studies agree that whitecaps dominate wave energy dissipation in conditions of young seas and high wind speeds. At lower wind speeds in swell-dominated seas, the combination of S_μ and S_{bg} can be much larger than S_{wcap}, but the precise relative magnitude of S_μ and S_{bg} is less certain.

The S_{wcap} term can be written as a function of S_{in}, S_{bg} and the fraction of the energy dissipation rate due to microscale breakers, Φ, as $S_{wcap} = \left(S_{in} - S_{bg}\right)(1 - \Phi)$. It is not the goal of this paper to resolve the relative magnitude of either S_μ or S_{bg}, but an attempt is made to evaluate the magnitude of their sum, $S_{other} = S_\mu + S_{bg}$. With this in mind, S_{wcap} is written as $S_{wcap} = S_{in} - S_{other}$. Now, W_{growth} and W are written in terms of S_{in} and S_{other} to give, respectively,

$$W_{growth} = \frac{S_{in} - S_{other}}{\Omega \rho \hat{z}_p^*}, \tag{19}$$

and

$$W = \frac{(S_{in} - S_{other})}{\Omega \rho \hat{z}_p^*}(1 + \delta). \tag{20a}$$

When the effects of surfactants are not important, equation (20a) becomes

$$W = \frac{(S_{in} - S_{other})}{\Omega \rho \hat{z}_p^*}(1 + \delta^*). \tag{20b}$$

4. Model Evaluation and Discussion

Using the model developed in section 3, this section explores the influence of variable $\hat{z}_p^*$ on both W_{growth} and W at a fixed value of S_{wcap}. Following this, a published field dataset of whitecap observations (Scanlon and Ward, 2016) is used to develop a parameterisation of $\hat{z}_p^*$

as a function of wind speed which is then used to estimate the magnitude of S_{wcap} from a set of whitecap coverage observations reported in Callaghan et al. (2008). The results are then used to determine the magnitude of S_{wcap}/S_{in} and compared to results from Banner and Morison (2018), based on the field dataset of Sutherland and Melville (2013, 2015).

4.1 Estimated Variation in W_{growth} due to $\hat{z}_p^*$

For a given value of S_{wcap}, equation (13) indicates that W_{growth} is inversely related to $\hat{z}_p^*$. This means that a measurement or estimate of W_{growth} alone is insufficient to infer a unique value of S_{wcap} because the average bubble plume penetration depth for a set of whitecaps may vary across different sea states. W_{growth} is a 2-D measurement of the 3-D breaking process in which the depth of the bubble plume is inextricably linked to the overall degree of energy loss. If an estimate of the bubble plume penetration depth is not combined with the surface 2-D W_{growth} expression, then W_{growth} alone cannot be faithfully used to estimate S_{wcap}, or vice-versa. In other words, while different distributions of whitecaps could potentially give the same value of W_{growth}, the whitecap distribution with the deepest bubble plumes would dissipate more wave energy, and therefore be associated with a larger value of S_{wcap}. This has important implications for how measurements of W_{growth} alone can be interpreted in terms of the energy dissipation rate associated with whitecaps.

As stated in section 3.1, $\hat{z}_p^*$ can be interpreted as an indicator of the dissipation rate of wave energy per unit whitecap area during active breaking, and plays a pivotal role in linking S_{wcap} and W_{growth}. This result is shown graphically in figure 2 for a fixed value of S_{wcap} and an arbitrary range of plume penetration depths extending from 5 cm to 50 cm. Here, W_{growth} has been normalized to its maximum value to highlight the relative change in

W_{growth} with increasing $\hat{z}_p^*$. It should be expected that $\hat{z}_p^*$ does not remain constant across all wind speeds and sea states as the scales (and possibly slopes) of breaking waves increase when sea states become more severe. Furthermore, because the rate of change of W_{growth} decreases as $\hat{z}_p^*$ increases, greater variability in W_{growth} may be expected when bubble plume penetration depths are small and variable (figure 2b). This implies that measurements of growth phase whitecap coverage would likely suffer more scatter at low values of S_{wcap}, something which has been found in field datasets (Scanlon et al. 2016).

4.2 Estimated Variation in W due to $\hat{z}_p^*$ and δ

As with W_{growth}, the value of W also depends on the average bubble plume penetration depth, as determined by equations (14) and (17). However, W is additionally dependent on W_{decay} whose magnitude relative to W_{growth} is given by δ, or δ^* when surfactant effects are absent or excluded. Therefore, the specific relationship between W and S_{wcap} is governed by the magnitude of $(1+\delta)/\hat{z}_p^*$ or $(1+\delta^*)/\hat{z}_p^*$. The terms $(1+\delta)/\hat{z}_p^*$ and $(1+\delta^*)/\hat{z}_p^*$ can be viewed as variable "constants" of proportionality that dictate how W and S_{wcap} are related.

W_{decay} is a function of both the length of time it takes a bubble plume to degas, which is dependent on $\hat{z}_p^*$, and surfactant-driven foam stabilization, with both of these effects encapsulated in δ. The decay phase of whitecap evolution will be extended for whitecaps that form deeper plumes, and W_{decay} therefore increases. In other words, increases in $\hat{z}_p^*$ lead to increases in δ. Furthermore, at a fixed value of S_{wcap}, any change in $\hat{z}_p^*$ requires a corresponding inverse change in W_{growth} to maintain the energy balance. For example, if $\hat{z}_p^*$ increases, fewer whitecaps are needed to maintain the energy balance with S_{wcap} due to their deeper bubble plume penetration depths, and W_{growth} must therefore decrease. The result is

an increase in W_{degas} that coincides with the decrease in W_{growth}, and this in turn increases δ. The coincident whitecap and ε observations of Schwendeman and Thomson (2015) show an increase in the lifetime of decaying whitecaps with an increase in measured ε, which they postulate to be associated with deeper bubble plume penetration. When surfactant effects are important, δ is also dependent on surfactant-driven foam stabilization. Following CDS17 it is assumed that surfactant effects do not significantly affect W_{growth} and only act to increase δ via the W_{stab} term in equation (15).

Ultimately, it is the combined effect of δ, δ^* and $\hat{z}_p^*$ that determine the relationship between whitecap coverage and the breaking wave energy dissipation rate and it is important to determine their expected inter-dependence. Figure 3 shows the relationship between $\hat{z}_p^*$ and both δ and δ^* for the oceanic whitecaps examined within the Callaghan et al. (2012) dataset. The Callaghan et al. (2012) dataset is hereafter referred to as the SPACE08 dataset, an acronym for the Surface Processes and Acoustics Communications Experiment which took place offshore of the Martha's Vineyard Coastal Observatory. The data are from four observational periods that correspond to different wind and wave conditions as described in Callaghan et al. (2012). By definition, δ^* does not contain any surfactant-driven foam stabilization effects, and should be entirely determined by $\hat{z}_p^*$. As expected, δ^* increases with increasing $\hat{z}_p^*$, in agreement with the physical argument set out in Monahan and O'Muircheartaigh (1986), the laboratory experiments of CDS16 and the inferences of Schwendeman and Thomson (2015). The $\delta^*(\hat{z}_p^*)$ relationship is well approximated by the following least-mean-squares best fit power law:

$$\delta^* = 8.65(\pm 5.38)\left(\hat{z}_p^*\right)^{0.69(\pm 0.30)} \tag{21}$$

with squared correlation coefficient $r^2 = 0.98$. Coefficients in parentheses represent 95% confidence intervals. This power law ensures that as $\hat{z}_p^*$ approaches zero, δ^* also approaches zero, which is what is physically expected. Also shown in figure 3 is the relationship between $\hat{z}_p^*$ and δ. Since δ includes additional information related to surfactant-driven foam stabilization, it is always greater than δ^*.

In the absence of the complicating effect of surfactants, the effect of the co-dependence of δ^* and $\hat{z}_p^*$ in setting the relationship between W and S_{wcap} is via equation (17), and this is illustrated in figure 4a. Here, a fixed value of S_{wcap} is used and equation (21) has been used to estimate δ^* for a range of values of $\hat{z}_p^*$. W has been normalized to its maximum value to highlight its relative change with increasing $\hat{z}_p^*$. Similarly to W_{growth} (figure 2a), W decreases as bubble plume penetration depth increases. However, because changes in $\hat{z}_p^*$ are also reflected in δ^*, the combined effect means the relative decrease in W is less in comparison to the decrease in W_{growth}. For an order of magnitude increase in $\hat{z}_p^*$, W decreases by about a factor of 3 from its maximum value, as compared to an order of magnitude reduction in W_{growth} over the same range of increasing $\hat{z}_p^*$. This effect is also reflected in the decrease in the gradient of W^* with increasing $\hat{z}_p^*$ shown in figure 4b, as compared to figure 2b. As with W_{growth}, greater variability in W may be expected for shallow and variable bubble plume penetration depths at low wind speeds, than for larger penetration depths expected at higher wind speeds, something which has been shown in many previous datasets (e.g. deLeeuw et al. 2011; Brumer et al. 2017).

The effect of surfactants to extend whitecap lifetime means that $(1 + \delta)/\hat{z}_p^*$ will always be equal to or larger than $(1 + \delta^*)/\hat{z}_p^*$. This can be seen in Table 1 which contains values of $\hat{z}_p^*$,

δ, δ^*, $(1+\delta)/\hat{z}_p^*$ and $(1+\delta^*)/\hat{z}_p^*$ estimated from the SPACE08 dataset, along with the measured wind speed, u_{10}. Furthermore, the particular field dataset presented here shows that $(1+\delta)/\hat{z}_p^*$ is less variable than $(1+\delta^*)/\hat{z}_p^*$. This is because the additional surfactant effect results in a quasi-linear $\delta(\hat{z}_p^*)$ relationship as seen in figure 3. In other words, for the SPACE08 dataset, both $\hat{z}_p^*$ and δ varied in a similar way, and the net result is an almost constant value of $(1+\delta^*)/\hat{z}_p^*$. This may not be the case for all field datasets and it is expected that differences between $(1+\delta)/\hat{z}_p^*$ and $(1+\delta^*)/\hat{z}_p^*$ will be dependent on local surfactant variability. If however the physical process of bubble plume degassing is broadly similar for whitecaps of similar dimensions, then the $\delta^*(\hat{z}_p^*)$ relationship given by equation (21) would be expected to exhibit less variability.

4.3 Using whitecap coverage to estimate $\hat{z}_p^*$, and S_{wcap}

4.3.1. Estimating $\hat{z}_p^*$

In order to estimate S_{wcap} from observations of whitecap coverage, the value of $\hat{z}_p^*$ must be constrained. While very little is known about $\hat{z}_p^*$ for actively breaking waves, measurements of the ratio W_{growth}/W can be used to provide a first-order estimate of $\hat{z}_p^*$, which, following equations (19) and (20b), is given by $W_{growth}/W = (1+\delta^*)^{-1}$. (Note that in using equation (20b) in place of equation (20a) it is assumed that W_{stab} is negligible). This is a useful result because it is seen that the W_{growth}/W ratio is independent of S_{wcap}, being only dependent on δ^*. Moreover, noting that δ^* is fundamentally dependent on $\hat{z}_p^*$ as discussed in section 3.1, measurements of W_{growth}/W can be used in conjunction with equation (21) to constrain the magnitude of $\hat{z}_p^*$, without *a priori* knowledge of S_{wcap}.

Scanlon and Ward (2016) report values of both W and stage A whitecap coverage, W_A, from the North Atlantic as a function of wind speed up to a maximum value of approximately 21 m/s. The ratio W_A/W from their field measurements is used here to approximate the ratio W_{growth}/W, such that $W_{growth} \approx W_A$. While W_{growth} and W_A are not identical, they can be assumed to be broadly analogous as they are both representations of the whitecap fraction associated with active air entrainment during wave breaking. This is a necessary approximation because extensive measurements of W_{growth}, as defined by equation (8a), have not been made. Note that it is assumed that $W_{degas} \gg W_{stab}$ for the W values in Scanlon and Ward (2016). These wind-speed dependent data are combined with equations (19) and (20b) to constrain the variability of $\hat{z}_p^*$ as a function of increasing wind speed as follows.

Figure 5 shows the W_{growth}/W data from Scanlon and Ward (2016), binned as a function of wind speed. The data decrease with increasing wind speed, which indicates that δ^* increases as a function of wind speed. An increase in δ^* implies an increase in W_{degas} relative to W_{growth} as a result of increases in bubble plume penetration depth. By adopting equation (21), the value of W_{growth}/W can therefore be used to infer $\hat{z}_p^*$, allowing a relationship between $\hat{z}_p^*$ and u_{10} to be developed. This has been done as described below.

A dimensionally consistent relationship between $\hat{z}_p^*$ and u_{10} of the form

$$\hat{z}_p^* = c_1 \frac{u_{10}^2}{g} + z_{p,o}, \qquad (22)$$

is adopted. c_1 is a non-dimensional scaling coefficient and $z_{p,o}$ is the minimum plume penetration depth for an air-entraining breaking wave, and is expected to be on the order of the diameter of the largest bubble entrained during breaking. Equation (22) was used to

calculate $\hat{z}_p^*$ for the wind speed values in figure 5a with different values of c_1 and $z_{p,o}$. The corresponding value of $\hat{z}_p^*$ was then converted to δ^* using equation (21), allowing the ratio W_{growth}/W to be calculated at each wind speed. This procedure produced multiple W_{growth}/W estimates as a function of wind speed, each from a unique c_1 and $z_{p,o}$ pair. The final values of c_1 and $z_{p,o}$ were found to be 0.0098 and 0.02 m, respectively, chosen to minimise the mean square error between the W_{growth}/W observations and the model W_{growth}/W values. The final W_{growth}/W curve is shown in figure 5a as the black line.

The ratio W_{growth}/W provides important information on whether or not it is physically reasonable to expect $\hat{z}_p^*$ to vary with changes in surface forcing and sea state. For example, if $\hat{z}_p^*$ is constant for all conditions, then the ratio W_{growth}/W should also be constant. The ratio W_{growth}/W is calculated assuming a fixed value of $\hat{z}_p^* = 0.15$ m and shown in figure 5a. The resulting straight line is not a good representation of the *in situ* measurements of Scanlon and Ward (2016).

The estimates of $\hat{z}_p^*$ as a function of u_{10} derived from the Scanlon and Ward (2016) data using the model developed here are shown in figure 5b. Also shown is equation (22), with appropriately chosen constants, c_1 and $z_{p,o}$. The dimensionally-consistent quadratic form of the relationship between $\hat{z}_p^*$ and u_{10} provides a good fit to the datapoints, and provides supporting evidence for an expected non-linear increase in bubble plume penetration depth as a function of increasing wind speed.

4.3.2. Estimating S_{wcap} from W and $\hat{z}_p^*$

The $\hat{z}_p^*(u_{10})$ relationship given in the previous section can now be used with equation (20b) to estimate S_{wcap} using field measurements of W. The particular whitecap dataset used is taken from Callaghan et al. (2008). This dataset is derived from over 43,000 digital sea-surface images collected in the North Atlantic in 2006 during the Marine Aerosol Production (MAP) field campaign. The dataset encompasses 107 W measurements made at u_{10} values between approximately 4 m/s to 23 m/s.

Figure 6a shows the relationship between u_{10} and S_{wcap} calculated from equation (20b), and figure 6b shows the same data binned in 1 m/s wind speed intervals. For comparison, two wind speed only parameterisations of total wave field energy dissipation rate are shown, which are taken from Hanson and Phillips (1999) and Hwang and Sletten (2008), hereafter referred to as HP99 and HS08, respectively. Both these previous relationships characterise $S_{diss}(u_{10})$, thereby implicitly including contributions from whitecaps, microscale breaking waves and other background processes.

The HP99 relationship was determined with the equilibrium range theory of Phillips (1985) which was applied to wind and wave field measurements to estimate S_{diss}. Within the scatter of the data, S_{diss} was found to be proportional to $u_{10}^{3.74}$, in agreement with the theoretical arguments of Wu (1988) who suggested that $S_{diss} \propto u_{10}^{3.75}$. Further, secondary dependencies of S_{diss} on wind history and wave field development were also found by HP99. For example, at a given wind speed S_{diss} was found to be systematically smaller in a rising wind than in a falling wind, highlighting the importance of the effects of wind-forcing over time-scales of several hours on local wave field energy dissipation.

The HS08 relationship was determined using a combination of analytical modelling and empirical relationships derived from observations. It predicts a linear relationship between wave field energy dissipation rate and the cube of the wind speed for an equilibrium sea state. The constant of proportionality was found to have a non-monotonic relationship with wave age, increasing with wave age for developing seas before reaching a peak and decreasing for older swell-dominated seas.

The ranges of S_{wcap} values in figure 6a covers more than 4 orders of magnitude ranging from 3×10^{-4} W m^{-2} at a wind speed of 4 m/s, to 6 W m^{-2} at a wind speed of approximately 23 m/s. These values of S_{wcap} are similar in range to the estimated dissipation rate due to all breaking waves reported in Sutherland and Melville (2015). It is clear that the non-linear dependence between S_{wcap} and u_{10} varies as a function of wind speed, as highlighted in figure 6a by the two grey lines which represent different wind speed dependencies. At lower wind speeds, the relative increase in S_{wcap} is much more rapid than at higher wind speeds, with an apparent transition in slope taking place at a wind speed of approximately 10 – 12 m/s. Potential reasons for this change in slope are discussed below in the context of the general conclusions of Sutherland and Melville (2015) and Banner and Morison (2018).

In an equilibrium sea state, it is expected that there is a balance between S_{in} and S_{diss}, where the latter may be the result of a combination of processes such as whitecapping (S_{wcap}), microscale breaking (S_{μ}) and other background dissipative processes (S_{bg}). While the exact relative magnitude of S_{wcap}, S_{μ} and S_{bg}, is not well constrained for all wind speeds and sea states, there is an emerging consensus that in young wind-driven seas at sufficiently large wind speeds, S_{wcap} is the dominant dissipative term (Sutherland and Melville, 2015; Banner and Morison, 2018). In these wind and wave conditions, the relative magnitude of both S_{μ}

and S_{bg} has been estimated to lie between about 20% (Sutherland and Melville, 2015) to only a few percent at most (Banner and Morison, 2018). Indeed, figure 13 and figure A2 in Banner and Morison (2018) suggest that above wind speeds of 12 m/s in developing seas, S_{wcap} accounts for upwards of 95% of S_{diss}. At lower wind speeds, in swell-dominated seas, the relative magnitude of both S_{μ} and S_{bg} increases, eventually dominating S_{wcap}.

Assuming an equilibrium wave field where $S_{diss} = S_{in}$, the agreement between the independent W-based estimate of S_{wcap} derived here, and the u_{10}-based estimate of S_{diss} from HP99 and HS08, also suggests that above wind speeds of 10 – 12 m/s, energy dissipation by whitecaps roughly balances wind energy input to the wave field on average. Deviations from this are expected due to variability in sea state at a given wind speed and are discussed further below. This overall result is in good agreement with the conclusions of Sutherland and Melville (2015) and Banner and Morison (2018). Moreover, this result, coupled with the good quantitative agreement with the results of HP99 and HS08 within this intermediate to high wind speed range, provides independent validation of the whitecap coverage dissipation model developed in section 3.1.

At wind speeds below approximately 10 m/s, the W-based S_{wcap} estimates begin to fall below the HP99 and HS08 parameterisations of S_{diss}, and consistently so at wind speeds below about 8 m/s (see figure 6). The implication is that at low wind speeds, when swell-dominated sea states are more common, the relative magnitude of S_{wcap} diminishes with decreasing wind speed, as the magnitude of S_{other} increases to maintain the balance between S_{diss} and S_{in}. Again, this is in agreement with the findings of both Sutherland and Melville (2015) and Banner and Morison (2018). Furthermore, an estimate of the magnitude of S_{wcap}/S_{in} as a function of wind speed for the Callaghan et al. (2008) W dataset can be made

and compared to the wind-speed dependent data presented in Banner and Morison (2018), and is achieved as follows.

For wind speeds above 12 m/s, an equilibrium wave field is assumed such that $S_{in} = S_{diss}$. Furthermore, following the data presented in figure 13 of Banner and Morison (2018), at these particular wind speeds it is also assumed that $S_{wcap} \gg S_{other}$ such that $S_{wcap} \approx S_{diss} = S_{in}$. Following HP99 and HS08, and employing the assumptions outlined above, a simple wind speed based estimate of S_{in} is derived from a least-mean squares fit of S_{wcap} and u_{10} over the wind speed range $12 \leq u_{10} \leq 23$ m/s. This gives the following power law relationship,

$$S_{in} = 1.11 \times 10^{-4} \, (\pm 1.22 \times 10^{-4}) u_{10}^{3.45 \, (\pm 0.36)}, \tag{23}$$

with squared correlation coefficient, r^2=0.88. This relationship is depicted as the black curve in figure 6b, and it is seen to lie between the HP99 and HS08 $S_{diss}(u_{10})$ curves. Extrapolating this curve to wind speeds below 12 m/s can provide a first-order estimate of S_{in} at these lower wind speeds allowing the magnitude of S_{wcap}/S_{in} to be computed.

The magnitude of S_{wcap}/S_{in}, averaged in 1 m/s wind speed bins, is shown in figure 7a. As expected, above wind speeds of 12 m/s, the S_{wcap}/S_{in} estimates are scattered around a value of unity, indicating that, on average, energy dissipation rate by whitecaps approximately balances wind energy input rate to the wave field. Below a wind speed of 10 m/s, however, the binned S_{wcap}/S_{in} values begin to systematically decrease, approaching 10 – 20% at wind speeds of 5 m/s. For comparison, S_{wcap}/S_{diss} data taken from figure 13 of Banner and Morison (2018) are also shown. In general, there is good agreement between the two datasets across the overlapping wind speed range. In particular, the two datasets show the same trend

at wind speeds below 10 - 12 m/s, with the relative contribution of S_{wcap} to S_{diss} decreasing with decreasing wind speed. Differences in absolute magnitude between the two datasets may be due to different sea state conditions encountered in the respective field campaigns, as well unaccounted-for deviations from the assumptions employed herein. Nevertheless, the agreement is encouraging, providing evidence of the decreasing contribution of S_{wcap} to S_{diss} at lower wind speeds, as well as demonstrating the usefulness of the W-based energy dissipation model that has been developed in this study.

As noted by HP99 and HS08, simple wind speed based parameterisations of wave processes such as wave energy dissipation may perform adequately in the mean, but will fail to capture the true natural variability associated with different sea states existing at similar wind speeds. This is because short term wind speed statistics do not necessarily reflect the prior wind history, an important factor controlling any given sea state. The S_{wcap}/S_{in} data used to produce the bin averages in figure 7a are now shown without bin-averaging in figure 7b. Each datapoint is derived from a single W value, and has been classified according to wind history in a manner similar to HP99. The wind acceleration was calculated as $\mathrm{a}_{u10} = \Delta\overline{u_{10}}/\Delta t$ where the overbar represents a 2.5 hour temporal average. Datapoints were classified as “rising” or “falling” for positive or negative values of a_{u10}, respectively, and the wind history classification is indicated in figure 7b.

At wind speeds above 10 m/s and below 6 m/s, there is a striking separation of S_{wcap}/S_{in} datapoints according to wind history. Within these wind speed regimes, S_{wcap}/S_{in} from falling winds generally lie above those from cases of rising winds. Furthermore, above $u_{10} \approx$ 12 m/s, where whitecaps are expected to almost completely balance the wind energy input to the wave field, the segregation of S_{wcap}/S_{in} datapoints occurs quite clearly at a value of

unity. In other words, on average, the dissipation rate of wave energy by whitecaps at a given wind speed appears to be greater in conditions of falling winds than in conditions of rising winds. The implication is that sea state development at a given wind speed drives much of the scatter in wind speed based estimates of wave field related parameters, something which has been explicitly shown in previous studies (e.g. Hanson and Phillips, 1999; Stramska and Petelski, 2003; Sugihara et al., 2007; Hwang and Sletten, 2008; Goddijn-Murphy et al., 2011; Sutherland and Melville, 2013, 2015; Brumer et al., 2017; Banner and Morison, 2018).

The wind history results presented here agree well with the findings of HP99. From their estimates of total wave field energy dissipation, HP99 found that for a given value of u_{10}, values of S_{diss} showed a negative correlation with wind acceleration. At a wind speed of 15 m/s, the relative differences were smaller but still present, with S_{diss} about a factor of 2-3 higher in falling winds than in rising winds. At a lower wind speed of 5 m/s, they found S_{diss} to be greater by up to a factor of 10 in falling winds than in rising winds (see their figure 9). Both the trend and magnitude of their results are echoed in figure 7b. Largest wind history differences of up to a factor of 10 in S_{wcap}/S_{in} occur at wind speeds in the range 4 – 6 m/s, reducing to about a factor of 2 for wind speeds higher than about 12 m/s.

Historically, datasets of whitecap coverage have shown a large degree of scatter when parameterised as a function of u_{10}. However, as shown in Brumer et al. (2017), wind speed parameterisations of whitecap datasets gathered since about 2004 show much better agreement, which is probably a reflection of the availability of much larger image datasets and improved digital image processing techniques. Brumer et al. (2017) state that many of these wind speed only parameterisations agree to within 30% of the ensemble mean value at wind speeds greater than 10 m/s. This may suggest that the impact of variations in sea state

on whitecap statistics are reduced at intermediate to high wind speeds. One possible explanation for this is that there is much less variation in S_{wcap}/S_{in} at these higher wind speeds. At lower wind speeds, the ratio S_{wcap}/S_{in} may be more susceptible to variations in sea state, especially when seas are often influenced by swell to a varying degree, thereby providing relatively larger variations in breaking statistics.

4.3.3 Variation in W and W_{growth} as a function of S_{wcap} and $\hat{z}_p^*$

The previous sections have demonstrated that whitecap coverage can vary at a given value of S_{in} through variations in S_{wcap}, S_{other}, and $\hat{z}_p^*$. Figure 8 shows how W_{growth} and W can vary as a function of S_{wcap} for varying values of $\hat{z}_p^*$, thus removing the complicating influence of varying magnitude of S_{other}. With a fixed value of $\hat{z}_p^*$, there is a linear relationship between S_{wcap} and both W and W_{growth}. The use of a variable $\hat{z}_p^*$, however, reduces the rate of increase of both W_{growth} and W with increasing S_{wcap}. The reduction is greater for W_{growth} than W because of the additional influence of $\hat{z}_p^*$ in setting the magnitude of the W_{degas} component of W (see section 3.1). This reduction in both W and W_{growth} provides a plausible physical explanation for the reported "levelling off" in whitecap coverage measurements at high wind speeds, especially when the contribution of foam streaks stabilized by surfactants are not considered (e.g., Nordberg et al., 1971; Ross and Cardone, 1974; Holthuijsen et al., 2012; Schwendeman et al., 2015; Brumer et al., 2017).

5. Summary and Concluding Remarks

There is a large body of both experimental and numerical evidence that the volume of the two-phase flow associated with whitecaps is closely related to the total energy dissipated during wave breaking (Duncan 1981; Lamarre and Melville 1991; Blenkinsopp and Chaplin 2007; Callaghan et al. 2016; Deane et al. 2016; Deike et al. 2016). Motivated by these results,

an energy-balance approach has been adopted to relate whitecap coverage (W), and growth phase whitecap coverage (W_{growth}), to the collective properties of individual whitecaps, and then to the energy dissipation rate associated with breaking wave whitecaps (S_{wcap}). This has resulted in mathematical relationships of W and W_{growth} developed here that account for growth phase whitecap coverage driven by air entrainment, as well as decay phase whitecap coverage driven by both bubble plume degassing and surfactant-driven foam stabilization.

An important finding is that neither W nor W_{growth} are likely to be uniquely related to S_{wcap} due to an additional dependency on the average bubble plume penetration depth for a given distribution of whitecaps ($\hat{z}_p^*$). By definition $\hat{z}_p^*$ is constant for any single set of whitecaps, but its value can vary between different sets of whitecaps. In addition, it is explicitly shown how surfactant-driven foam stabilization is also important for W, but not for W_{growth}. A linear relationship between the two-dimensional surface W or W_{growth}, and the three-dimensional quantity S_{wcap}, may only be expected if all distributions of whitecaps have the same average bubble plume penetration depth. This seems unlikely given the large variation in sea state and breaking wave scale (and possibly slope) across the global oceans. Furthermore it is not supported by observations of individual oceanic whitecaps used to infer $\hat{z}_p^*$ from whitecap foam degassing times presented here. Moreover, laboratory breaking waves of varying slope and intensity generate variable bubble plume penetration depths.

Having an estimate of $\hat{z}_p^*$ is an essential component of any attempt to estimate S_{wcap} from measurements of either W or W_{growth}. The energy-balance model developed here was used in conjunction with the field data of Scanlon and Ward (2016) to calculate a relationship between $\hat{z}_p^*$ and u_{10}. Subsequent estimates of S_{wcap} as a function of u_{10} were made using $\hat{z}_p^*$

and measurements of W from Callaghan et al (2008). Under the assumption of an equilibrium sea state (i.e. $S_{in} = S_{diss}$), the resulting estimates of S_{wcap} suggest that at wind speeds above 12 m/s, the rate of wind energy input to the wave field is almost entirely balanced by breaking wave whitecaps. At lower wind speeds, the magnitude of S_{wcap} decreases rapidly with decreasing wind speed and drops well below two existing wind-speed based parameterizations for total wave energy dissipation. The difference between S_{wcap} and S_{diss} grows with decreasing wind speed. These two findings are in good agreement with the overall conclusions of Sutherland and Melville (2015) and Banner and Morison (2018): at higher wind speeds in young wind-driven sea states, whitecaps are the dominant mechanism for dissipation wind to wave energy input, while at lower wind speeds the relative importance of whitecaps diminishes and other background processes and possibly microscale breaking waves begin to dominate.

The development of simple mathematical expressions for W and W_{growth} provide a useful framework within which scatter within and between whitecap coverage datasets can be understood, and therefore how measurements and parameterisations of whitecaps can be used to estimate air-sea exchange processes. For example, more variability in W should be expected at low wind speeds due to the greater sensitivity between W and $\hat{z}_p^*$ when the latter is small. Furthermore, because deeper bubble plumes take longer to degas, this has a direct impact on the magnitude of W for a given value of S_{wcap}. Moreover, since W and W_{growth} are 2-dimensional measurements, neither can be used to uniquely quantify the volume of air entrained by breaking waves, unless accompanied by measurements or estimates of $\hat{z}_p^*$. While $\hat{z}_p^*$ has been parameterized here in terms of wind speed, it is presumably also a function of sea state, and wave slope in particular. Understanding the range of physical factors that affect W

is of fundamental importance to parameterizing air-sea exchange processes such as bubble-mediated gas exchange and sea spray aerosol flux as functions of W.

The present work supports taking a whitecap-by-whitecap approach to quantifying whitecap coverage and energy dissipation associated with whitecaps, and appropriate detailed measurements should be encouraged alongside traditional measurements of total whitecap coverage, and the more recent but increasingly common measurements of the Phillips distribution of breaking crest lengths (Phillips, 1985).

Acknowledgements

AHC acknowledges many fruitful discussions on breaking waves with Grant Deane and Dale Stokes. AHC is a Royal Society Shooter International Fellow funded by Prof. E. Shooter. Funding from U.S. NSF Grant OCE-1434866 is gratefully acknowledged. Dr. James Preisig is acknowledged for his considerable efforts running the SPACE08 campaign which was funded by the U.S. Office of Naval Research grants N00014-11-1-0158, N00014-10738, and N00014-11030. Data used in this paper will be made publicly available on figshare.com. The comments from the anonymous reviewers improved the manuscript throughout the review process.

Appendix A

A glossary of all mathematical variables and symbols used.

Table A1 here.

References

Anguelova, M. D., and F.Webster, 2006: Whitecap coverage from satellite measurements: A first step toward modeling the variability of oceanic whitecaps, J. Geophys. Res., 111, C03017, doi:10.1029/2005JC003158.

Anguelova, M. D., and P. A. Hwang, 2016: Using Energy Dissipation Rate to Obtain Active Whitecap Fraction. J. Phys. Oceanogr., 46, 461-481.

Ardhuin, F., B. Chapron, and F. Collard, 2009: Observation of swell dissipation across oceans. Geophys. Res. Lett., 36, L21608, doi:10.1029/2006GL027050.

Banner, M. L., and R. P. Morison, 2010: Refined source terms in wind wave models with explicit wave breaking prediction. Part I: Model framework and validation against field data. Ocean Modelling, 33, 177-189.

Banner, M. L., and R. P. Morison, 2018: On the upper ocean turbulent dissipation rate due to microscale breakers and small whitecaps. Ocean Modelling, 126, 63-76.

Banner, M. L., and O. Phillips, 1974: On the incipient breaking of small scale waves. J. of Fluid Mech., 65, 647-656.

Belcher, S. E., and Coauthors, 2012: A global perspective on Langmuir turbulence in the ocean surface boundary layer. Geophys. Res. Lett., 39, 10.1029/2012GL052932.

Bell, T. G., Landwehr, S., Miller, S. D., de Bruyn, W. J., Callaghan, A. H., Scanlon, B., Ward, B., Yang, M., and Saltzman, E. D., 2017: Estimation of bubble-mediated air/sea gas exchange from concurrent DMS and CO_2 transfer velocities at intermediate-high wind speeds, Atmos. Chem. Phys., 17, 9019–9033.

Blenkinsopp, C., and J. Chaplin, 2007: Void fraction measurements in breaking waves. Proc. R. Soc. A, 463, 3151-3170, doi:10.1098/rspa.2007.1901.

Bondur, V., and E. Sharkov, 1982: Statistical properties of whitecaps on a rough sea. Oceanology, 22, 274-279.

Brumer, S. E., Zappa, C. J., Brooks, I. M., Tamura, H., Brown, S. M., Blowquist, B. W., Fairall, C. W., and A. Cifuentes-Lorenzen, 2017: Whitecap coverage dependence on wind and wave statistics as observed during SO GasEx and HiWinGS, J. Phys. Oceanogr., 47, 2211-2235, doi: 10.1175/JPO-D-17-0005.1.

Callaghan, A. H., 2013: An improved whitecap timescale for sea spray aerosol production flux modeling using the discrete whitecap method. J. Geophys. Res.: Atmospheres, 118, 1-14, doi:10.1002/jgrd.50768.

Callaghan, A., G. de Leeuw, L. Cohen, and C. D. O'Dowd, 2008: Relationship of oceanic whitecap coverage to wind speed and wind history. Geophys. Res. Lett., 35, doi:10.1029/2008GL036165.

Callaghan, A. H., and M. White, 2009: Automated processing of sea surface images for the determination of whitecap coverage. J. Atmos. Oceanic Technol., 26, 383–394, doi:10.1175/2008JTECHO634.1.

Callaghan, A. H., G. B. Deane, and M. D. Stokes, 2013: Two regimes of laboratory whitecap foam decay: Bubble-plume controlled and surfactant stabilized. J. Phys. Oceanogr., 43, 1114-1126, DOI: 10.1175/JPO-D-12-0148.1.

Callaghan, A. H., G. B. Deane, and M. D. Stokes, 2016: Laboratory air-entraining breaking waves: Imaging visible foam signatures to estimate energy dissipation. Geophy. Res. Lett., 43, doi:10.1002/2016GL071226.

Callaghan, A. H., G. B. Deane, and M. D. Stokes, 2017: On the imprint of surfactant-driven stabilization of laboratory breaking wave foam with comparison to oceanic whitecaps, J. Geophys. Res. Oceans, 122, doi: 10.1002/2017JC012809

Callaghan, A. H., G. B. Deane, M. D. Stokes, and B. Ward, 2012: Observed variation in the decay time of oceanic whitecap foam. J. Geophys. Res.: Oceans, 117.

Cavaleri, L., and Coauthors, 2007: Wave modelling–the state of the art. Prog. in Oceanogr., 75, 603-674, doi:10.1016/j.pocean.2007.05.005.

De Leeuw, G., E. L. Andreas, M. D. Anguelova, C. W. Fairall, E. R. Lewis, C. D. O'Dowd, M. Schultz, S. E. Schwartz, 2011: Production flux of sea spray aerosol. Rev. of Geophys., 4 9, RG2001, doi:10.1029/2010RG000349.

Deane, G. B., M. D. Stokes, and A. H. Callaghan, 2016: The saturation of fluid turbulence in breaking laboratory waves and implications for whitecaps. J. Phys. Oceanogr., 46, 975-992, DOI: 10.1175/JPO-D-14-0187.1.

Deike, L., W. K. Melville, and S. Popinet, 2016: Air entrainment and bubble statistics in breaking waves. J. Fluid Mech., 801, 91-129, doi:10.1017/jfm.2016.372.

Derakhti, M. and J. T. Kirby, 2014: Bubble entrainment and liquid-bubble interaction under unsteady breaking waves. J. Fluid Mech., 761, 464-506.

Derakhti, M. and J. T. Kirby, 2016: Breaking-onset, energy and momentum flux in unsteady focused wave packets. J. Fluid Mech., 790, 553-581.

Duncan, J., 1981: An experimental investigation of breaking waves produced by a towed hydrofoil. Proc. R. Soc. A, 377, No. 1770, 331-348.

Fairall, C. W., M. Yang, L. Bariteau, J. B. Edson, D. Helmig, W. McGillis, S. Pezoa, J. E. Hare, B. Huebert, and B. Blomquist, 2011: Implementation of the Coupled Ocean-Atmosphere Response Experiment flux algorithm with CO_2, dimethyl sulfide, and O_3, J. Geophys. Res., 116, C00F09, doi:10.1029/2010JC006884.

Frouin, R., S. F. Iacobellis, and P. Y. Deschamps, 2001: Influence of oceanic whitecaps on the Global Radiation Budget. Geophys. Res. Lett., 28, 1523-1526.

Gemmrich, J., C. J. Zappa, M. L. Banner, and R. P. Morison, 2013: Wave breaking in developing and mature seas, J. Geophys. Res. Oceans, 118, 4542–4552, doi:10.1002/jgrc.20334.

Goddijn-Murphy, L., D. K. Woolf, and A. H. Callaghan, 2011: Parameterizations and algorithms for oceanic whitecap coverage. J. Phys. Oceanogr., 41, 742-756, doi: 10.1175/2010JPO4533.1.

Goddijn-Murphy, L., D. K. Woolf, A. H. Callaghan, P. D. Nightingale, and J. D. Shutler, 2016: A reconciliation of empirical and mechanistic models of the air-sea gas transfer velocity, J. Geophys. Res. Oceans, 121, 818–835, doi:10.1002/2015JC011096.

Gordon, H. R., 1997: Atmospheric correction of ocean color imagery in the Earth Observing System era. J. Geophys. Res., 102 (D14), 17 081–17 106.

Grythe, H., J. Ström, R. Krejci, P. Quinn, and A. Stohl, 2014: A review of sea-spray aerosol source functions using a large global set of sea salt aerosol concentration measurements, Atmos. Chem. Phys., 14(3), 1277–1297, doi:10.5194/acp-14-1277-2014.

Hanson, J. L. and O. M. Phillips, 1999: Wind sea growth and dissipation in the open ocean. J. Phys. Oceanogr., 29, 1633-1648.

Holthuijsen, L. H., M. D. Powell and J. D. Pietrzak, 2012: Wind and waves in extreme hurricanes, J. Geophys. Res., 117, C09003, doi:10.1029/2012JC007983.

Hwang, P. A., and M. A. Sletten, 2008: Energy dissipation of wind-generated waves and whitecap coverage. J. Geophys. Res.: Oceans, 113, C02012, doi:10.1029/2007JC004277.

Jessup, A., C. J. Zappa, and H. Yeh, 1997: Defining and quantifying microscale wave breaking with infrared imagery. J. Geophys. Res.: Oceans, 102, 23145-23153.

Kleiss J. M. and W. K. Melville, 2011: The analysis of sea surface imagery for whitecap kinematics. J. Atmospheric and Oceanic Technology, 28, 219-243, doi: 10.1175/2010JTECHO744.1.

Kraan, G., W. Oost, and P. Janssen, 1996: Wave energy dissipation by whitecaps. J. Atmospheric and Oceanic Technology, 13, 262-267.

Lamarre, E., and W. Melville, 1991: Air entrainment and dissipation in breaking waves. Nature, 351, 469.

Leckler, F., F. Ardhuin, J.-F. Filipot, and A. Mironov, 2013: Dissipation source terms and whitecap statistics. Ocean Modelling, 70, 62-74.

Melville, W. K., 1996: The role of surface-wave breaking in air-sea interaction. Ann. Rev. of Fluid Mech, 28, 279-321.

Monahan, E. C., 1971: Oceanic whitecaps. J. Phys. Oceanogr., 1, 139-144.

Monahan, E. C., D. E. Spiel, and K. L. Davidson, 1986: A model of marine aerosol generation via whitecaps and wave disruption, in Oceanic Whitecaps and Their Role in Air-Sea Exchange Processes, edited by E. C. Monahan and G. MacNiocaill, pp. 167‑174, D. Reidel, Dordrecht, Netherlands.

Monahan, E. C. and D. K. Woolf, 1989: Comments on ‘‘Variations of whitecap coverage with wind stress and water temperature.’’ J. Phys. Oceanogr., 19, 706–709.

Monahan, E. C., and I. G. O'Muircheartaigh, 1986: Whitecaps and the passive remote sensing of the ocean surface. Int. J. Remote Sensing, 7, 627-642.

Na, B., K.-A. Chang, Z.-C. Huang, and H.-J. Lim, 2016: Turbulent flow field and air entrainment in laboratory plunging breaking waves, J. Geophys. Res. Oceans, 121, 2980–3009, doi:10.1002/2015JC011377.

Nordberg, W., J. Conaway, D. B. Ross, and T. Wilheit, 1971: Measurements of microwave emission from a foam-covered, wind-driven sea, J. Atmos. Sci., 28, 429–435.

Oakey, N., and J. Elliott, 1982: Dissipation within the surface mixed layer. J. Phys. Oceanogr., 12, 171-185.

Phillips, O. M., 1985: Spectral and statistical properties of the equilibrium range in wind-generated gravity waves, J. Fluid Mech., 156, 505-531.

Quilfen, Y., C. Prigent, B. Chapron, A. A. Mouche, and N. Houti, 2007: The potential of QuikSCAT and WindSat observations for the estimation of sea surface wind vector under severe weather conditions. J. Geophys. Res., 112, C09023, doi:10.1029/2007JC004163.

Ross, D. B., and V. Cardone, 1974: Observations of oceanic whitecaps and their relation to remote measurements of surface wind speed. J. Geophys. Res., 79, 444-452.

Scanlon, B., Ø. Breivik, J.-R. Bidlot, P. A. Janssen, A. H. Callaghan, and B. Ward, 2016: Modeling Whitecap Fraction with a Wave Model. J. Phys. Oceanogr., 46, 887-894.

Scanlon, B. and B. Ward, 2016: The influence of environmental parameters on active and maturing oceanic whitecaps. J. Geophys. Res. Oceans, 121, 3325-3336, doi:10.1002/2015JC011230.

Schwendeman, M., and J. Thomson, 2015: Observations of whitecap coverage and the relation to wind stress, wave slope, and turbulent dissipation. J. Geophys. Res.: Oceans, 120, 8346–8363, doi:10.1002/ 2015JC011196.

Sharkov, E. A., 2007: Breaking ocean waves: geometry, structure and remote sensing. Springer Science & Business Media.

Stramska, M., and T. Petelski, 2003: Observations of oceanic whitecaps in the north polar waters of the Atlantic, J. Geophys. Res., 108(C3), 3086, doi:10.1029/2002JC001321.

Sutherland, P., and W. K. Melville, 2013: Field measurements and scaling of ocean surface wave-breaking statistics. Geophys. Res. Lett., 40, 1–6, doi:10.1002/grl.50584.

Sutherland, P., and W. K. Melville, 2015: Field measurements of surface and near-surface turbulence in the presence of breaking waves. J. Phys. Oceanogr., 45, 943-965, DOI: 10.1175/JPO-D-14-0133.1.

Thomson, J., E. A. D’ Asaro, M. F. Cronin, W. E. Rogers, R. R. Harcourt, and A. Shcherbina, 2013: Waves and the equilibrium range at Ocean Weather Station P, J. Geophys. Res. Oceans, 118, 5951‑5962, doi:10.1002/2013JC008837.

Thomson, J., M. S. Schwendeman, S. F. Zippel, S. Moghimi, J. Gemmrich, and W. E. Rogers, 2016: Wave-breaking turbulence in the ocean surface layer. J. Phys. Oceanogr., 46, 1857-1870, DOI: 10.1175/JPO-D-15-0130.1.

Thorpe, S. A., 2005: The turbulent ocean. Cambridge University Press.

Updegraff, G. E., and V. C. Anderson, 1991: Bubble noise and wavelet spills recorded 1 m below the ocean surface. J. Acoust. Soc. Am., 89(5), 2264-2279, doi: 10.1121/1.400917

Woolf, D. K., 2005: Parameterization of gas transfer velocities and sea-state-dependent wave breaking. Tellus, 57B, 87–94.

Wu, J., 1979: Oceanic whitecaps and sea state. J. Phys. Oceanogr., 9, 1064-1068.

Wu, J., 1988: Variations of whitecap coverage with wind stress and water temperature. J. Phys. Oceanogr., 18, 1448-1453.

Zhao, Z., E. A. D'Asaro and J. A. Nystuen, 2014: The sound of tropical cyclones. J. Phys. Oceanogr., 44, 2763-2778.

Tables

Table 1. Estimates of $\hat{z}_p^*$, δ, δ^*, $(1+\delta)\hat{z}_p^*$ and $(1+\delta^*)\hat{z}_p^*$, for 4 observational periods from the SPACE08 field dataset, along with wind speed for each period, u_{10}.

u_{10}[m/s]	$\hat{z}_p^*$ [m]	δ [−]	δ^* [−]	$(1+\delta)/\hat{z}_p^*$	$(1+\delta^*)/\hat{z}_p^*$
11.3	0.14	3.81	2.24	34.36	23.14
8.3	0.15	4.19	2.30	34.60	22.00
5.7	0.09	1.93	1.61	32.56	29.00
13.7	0.12	3.26	1.97	35.50	24.75

Table A1. Glossary of mathematical variables and symbols used.

Symbol	Description	Units
a_{u10}	Wind acceleration	m s^{-2}
A_{obs}	Observational area	m^2
$A(t)$	Time evolving whitecap foam area	m^2
$A_{GD}(t)$	Evolving whitecap foam area free from surfactant effects	m^2
A_o	Maximum whitecap foam area	m^2
S_{bg}	Energy dissipation rate due to background processes	W m^{-2}
S_{diss}	Total wave field energy dissipation rate	W m^{-2}
S_{in}	Wind to wave energy input flux	W m^{-2}
S_μ	Energy dissipation rate due to microscale breakers	W m^{-2}
S_{other}	$S_{bg} + S_\mu$	W m^{-2}
S_{wcap}	Whitecap driven wave energy dissipation rate	W m^{-2}
t	Time	s
t_{Ao}	Time of occurrence of A_o	s
T_{obs}	Observational time period	s
T_p	Peak spectral period	s
u_{10}	10 m wind speed	m s^{-1}
W	Total whitecap foam coverage	[-]
W_{meas}	Measured whitecap foam coverage	[-]

W_{growth}	Growth phase whitecap foam coverage	[-]
W_{decay}	Decay phase whitecap foam coverage	[-]
W_{degas}	Degassing phase whitecap foam coverage	[-]
W_{stab}	Surfactant stabilized whitecap foam coverage	[-]
W_A	Stage A whitecap foam coverage	[-]
W^*	Normalized whitecap foam coverage	[-]
W^*_{growth}	Normalized growth phase whitecap foam coverage	[-]
$\hat{z}_p$	Area-weighted bubble plume penetration depth	m
$\hat{z}^*_p$	Ensemble average growth-phase weighted $\hat{z}_p$	m
χ_{growth}	Whitecap growth phase area-time-integral	m^2 s
χ_{decay}	Whitecap decay phase area-time-integral	m^2 s
χ_{degas}	Whitecap degassing phase area-time-integral	m^2 s
χ_{stab}	Surfactant-driven foam stabilization area-time-integral	m^2 s
ϵ	Dissipation rate of turbulent kinetic energy	m^2 s^{-3}
δ	Ratio of W_{decay} to W_{growth}	[-]
δ^*	Ratio of W_{degas} to W_{growth}	[-]
ΔE_T	Total breaking wave energy dissipation	kg m^2 s^{-2}
ϕ	Fraction of S_{brk} dissipated by microscale breaking waves	[-]
Γ	Whitecap measurement efficiency	[-]
Ω	Turbulence strength parameter	m^2 s^{-3}
ρ	Seawater density	kg m^{-3}
ρ_a	Air density	kg m^{-3}
τ_{decay}	Characteristic total whitecap decay timescale	s
τ_{degas}	Characteristic whitecap degassing timescale	s
τ_{div}	Divergence timescale	s
τ_{growth}	Characteristic whitecap growth timescale	s
τ_{stab}	Characteristic whitecap stabilization timescale	s
Θ	Foam stabilization factor	[-]

Figure Captions

Figure 1. The open circles show the measured foam area time series of an oceanic whitecap from the SPACE08 dataset. The black curve is the estimated foam evolution in the absence of surfactant-effects which is found following the method described in Callaghan et al. (2017). The left-hand vertical dashed grey line marks the time ($t = t_{Ao}$) of the transition from the growth to decay phases of whitecap foam evolution, when the maximum foam area (A_o) is reached. The right-hand dashed grey line marks the time ($t = \tau_{div}$) of the transition from universal foam decay to surfactant-stabilized foam decay when surfactant effects are present and become important.

Figure 2(a,b). Panel a shows the variation in W_{growth} normalized by its maximum value (W^*_{growth}) as a function of $\hat{z}^*_p$ for a fixed value ofS_{wcap}. Panel b shows the rate of change of W^*_{growth} with increasing $\hat{z}^*_p$.

Figure 3. The relationship between the mean bubble plume penetration depth, $\hat{z}^*_p$, δ (circles), and δ^* (squares), calculated with the SPACE08 dataset. The solid line is a power law fit to the δ^* data, given by equation (21) in the main text.

Figure 4(a,b). Panel (a) shows the variation in normalized whitecap coverage (W^*) as a function of increasing bubble plume depth ($\hat{z}^*_p$) for a fixed value of S_{wcap}, following equation (17). Panel (b) shows the gradient in W^* as a function of $\hat{z}^*_p$. Notably, W^* shows less variation than W^*_{growth} for the same range in $\hat{z}^*_p$ shown in figure 2.

Figure 5(a,b). The datapoints in panel a show the relationship between measured W_A/W and u_{10} from the Scanlon and Ward (2016) where the approximation $W_{growth} \approx W_A$ has been

made. The dashed line is the model estimate of W_{growth}/W with a constant value of $\hat{z}_p^* =$ 0.15 m. The curved line incorporates a wind speed dependent estimate of $\hat{z}_p^*$ into the W_{growth}/W calculation following equation (22). Panel b plots the value of $\hat{z}_p^*$ estimated from the W_A/W measurements of Scanlon and Ward (2016). The black curve is equation (22).

Figure 6(a,b). Panel a shows the values of the energy dissipate rate due to whitecaps, S_{wcap}, as a function of wind speed, derived from measurements of whitecap coverage made during the MAP field campaign (Callaghan et al., 2008). Two different two wind speed power laws are indicated by the grey curves to highlight the different wind speed-dependent variability in the S_{wcap} estimates for high and low wind speeds. Panel b show the same dataset averaged into 1 m/s wind speed bins. Also shown are estimates of the total wave field energy dissipation rate, S_{diss}, from Hanson and Phillips (1999) (blue curve) and Hwang and Sletten (2008) (red curve). The black curve is an estimate of the rate of energy input to the wave field, S_{in}, from this study (see the main text for specific details on its formulation).

Figure 7(a,b). Panel a shows 1 m/s bin average values of the ratio of energy dissipation rate due to whitecaps, S_{wcap}, to the energy input rate from the wind to the wave field, S_{in}, as a function of wind speed. The S_{wcap} values were estimated using the MAP whitecap coverage dataset from Callaghan et al. (2008) in the context of the energy dissipation based model of whitecap coverage developed in this study. The additional black datapoints are similar estimates taken from figure 13 of Banner and Morison (2018), which were derived from the dataset of Sutherland and Melville (2015). Panel b shows the MAP-derived dataset in panel a, but without bin-averaging. The individual datapoints are classified as either from rising wind conditions (red circles) or falling wind conditions (blue circles), as determined from a wind acceleration analysis detailed in the main text.

Figure 8(a-b). Panel a shows the variation of W and W_{growth} as a function of S_{wcap} for different values of $\hat{z}_p^*$. The solid lines assume a constant value of 0.15 m. The dashed lines assume a variable $\hat{z}_p^*$ following equation (22) . Panel b shows the specific values of $\hat{z}_p^*$ for the S_{wcap} values used.

Figures

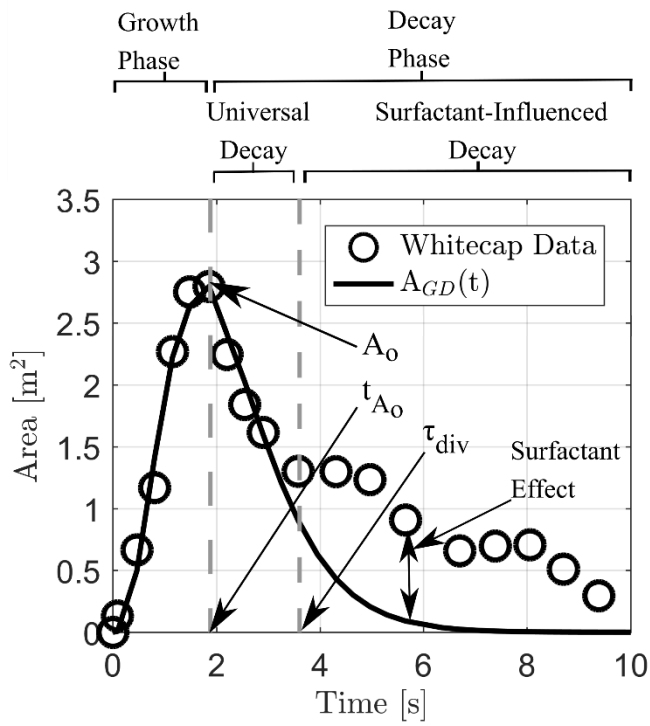

Figure 1. The open circles show the measured foam area time series of an oceanic whitecap from the SPACE08 dataset. The black curve is the estimated foam evolution in the absence of surfactant-effects which is found following the method described in Callaghan et al. (2017). The left-hand vertical dashed grey line marks the time ($t = t_{Ao}$) of the transition from the growth to decay phases of whitecap foam evolution, when the maximum foam area (A_o) is reached. The right-hand dashed grey line marks the time ($t = \tau_{div}$) of the transition from universal foam decay to surfactant-stabilized foam decay when surfactant effects are present and become important.

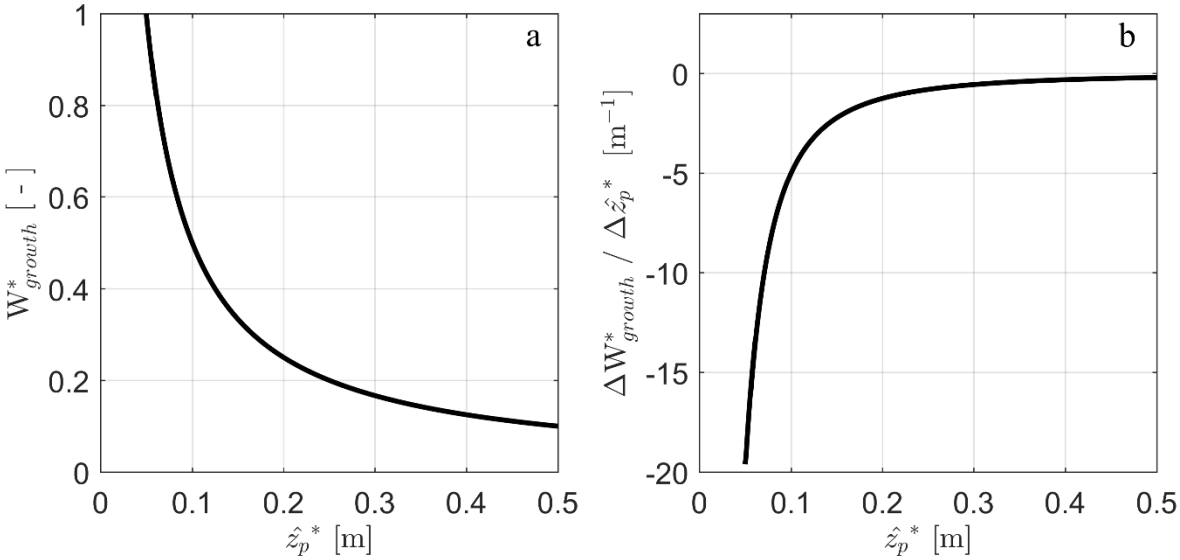

Figure 2(a,b). Panel a shows the variation in W_{growth} normalized by its maximum value (W^*_{growth}) as a function of $\hat{z}_p^*$ for a fixed value of S_{wcap}. Panel b shows the rate of change of W^*_{growth} with increasing $\hat{z}_p^*$.

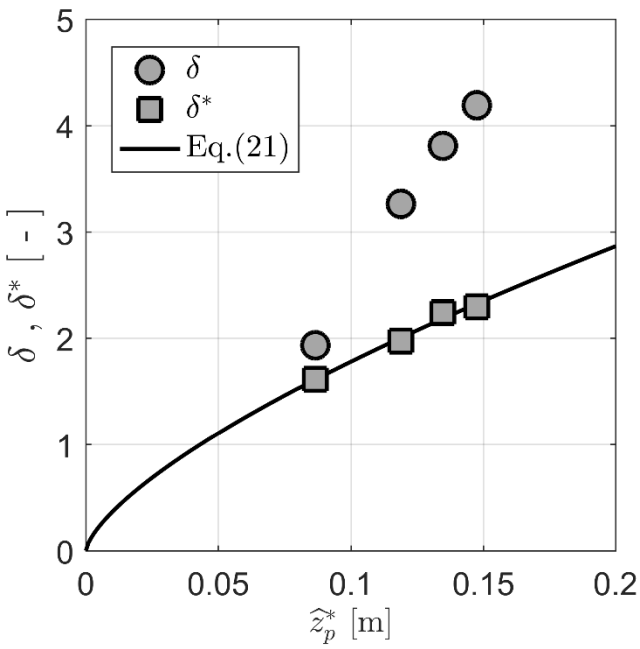

Figure 3. The relationship between the mean bubble plume penetration depth, $\hat{z}_p^*$, δ (circles), and δ^* (squares), calculated with the SPACE08 dataset. The solid line is a power law fit to the δ^* data, given by equation (21) in the main text.

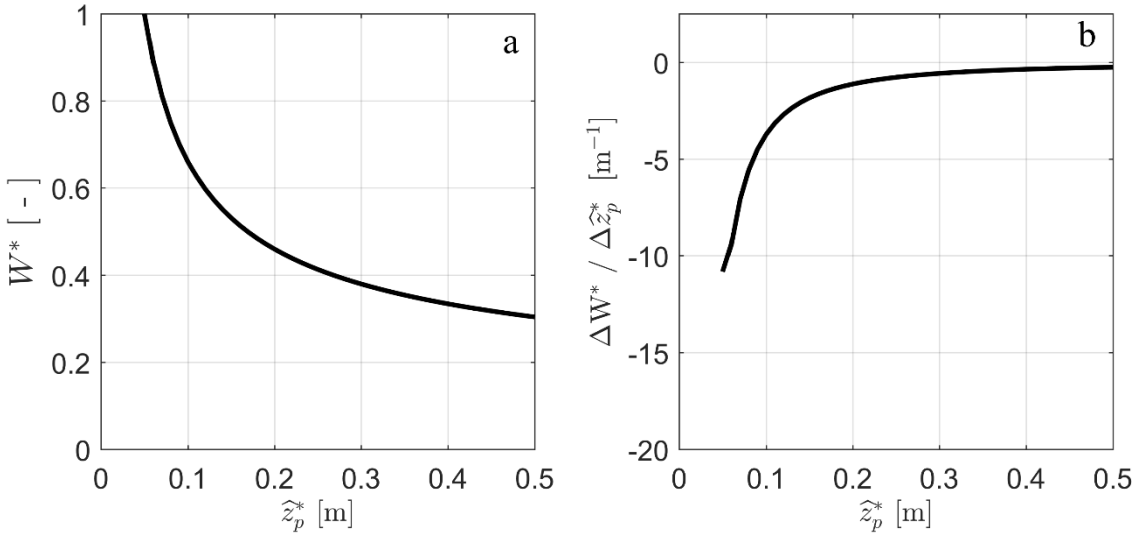

Figure 4(a,b). Panel (a) shows the variation in normalized whitecap coverage (W^*) as a function of increasing bubble plume depth ($\hat{z}_p^*$) for a fixed value of S_{wcap}, following equation (17). Panel (b) shows the gradient in W^* as a function of $\hat{z}_p^*$. Notably, W^* shows less variation than W_{growth}^* for the same range in $\hat{z}_p^*$ shown in figure 2.

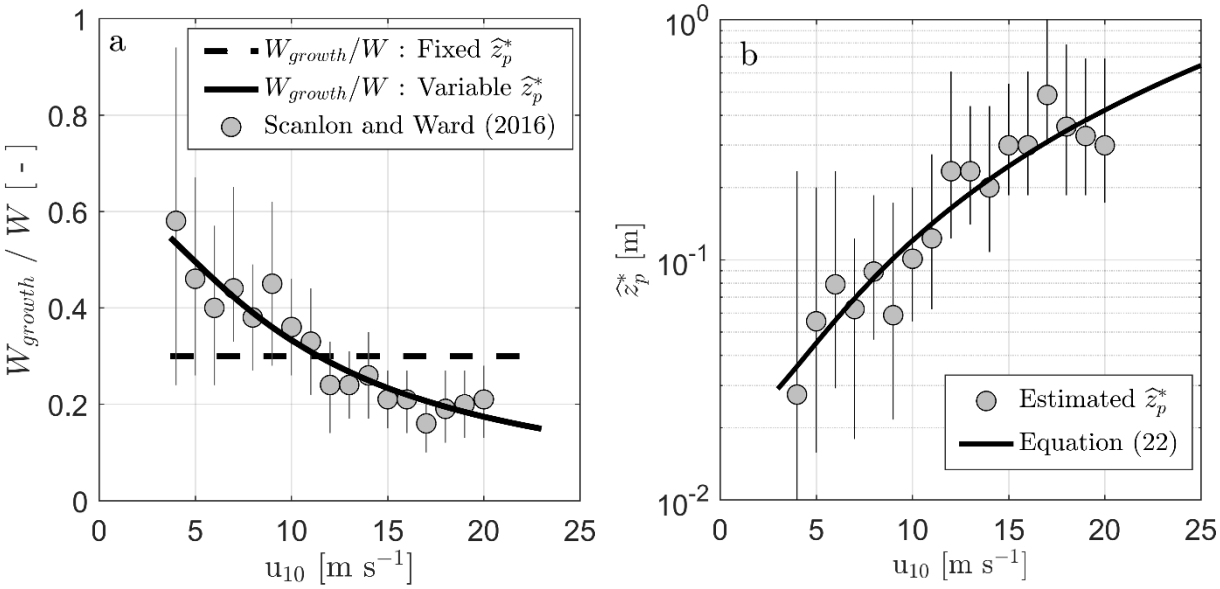

Figure 5(a,b). The datapoints in panel a show the relationship between measured W_A/W and u_{10} from the Scanlon and Ward (2016) where the approximation $W_{growth} \approx W_A$ has been made. The dashed line is the model estimate of W_{growth}/W with a constant value of $\hat{z}_p^* =$ 0.15 m. The curved line incorporates a wind speed dependent estimate of $\hat{z}_p^*$ into the W_{growth}/W calculation following equation (22). Panel b plots the value of $\hat{z}_p^*$ estimated from the W_A/W measurements of Scanlon and Ward (2016). The black curve is equation (22).

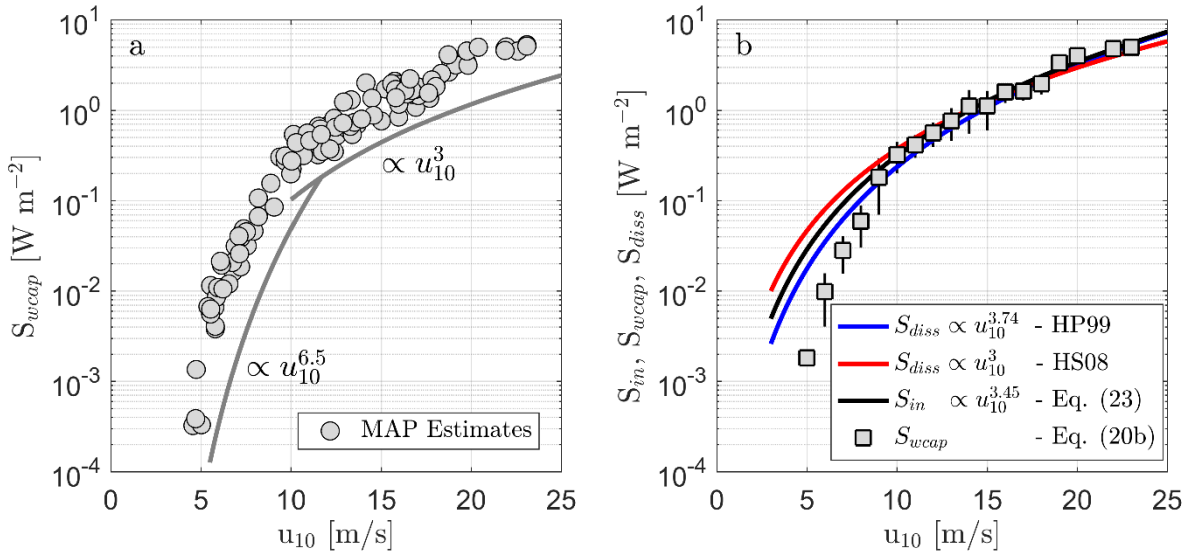

Figure 6(a,b). Panel a shows the values of the energy dissipate rate due to whitecaps, S_{wcap}, as a function of wind speed, derived from measurements of whitecap coverage made during the MAP field campaign (Callaghan et al., 2008). Two different two wind speed power laws are indicated by the grey curves to highlight the different wind speed-dependent variability in the S_{wcap} estimates for high and low wind speeds. Panel b show the same dataset averaged into 1 m/s wind speed bins. Also shown are estimates of the total wave field energy dissipation rate, S_{diss}, from Hanson and Phillips (1999) (blue curve) and Hwang and Sletten (2008) (red curve). The black curve is an estimate of the rate of energy input to the wave field, S_{in}, from this study (see the main text for specific details on its formulation).

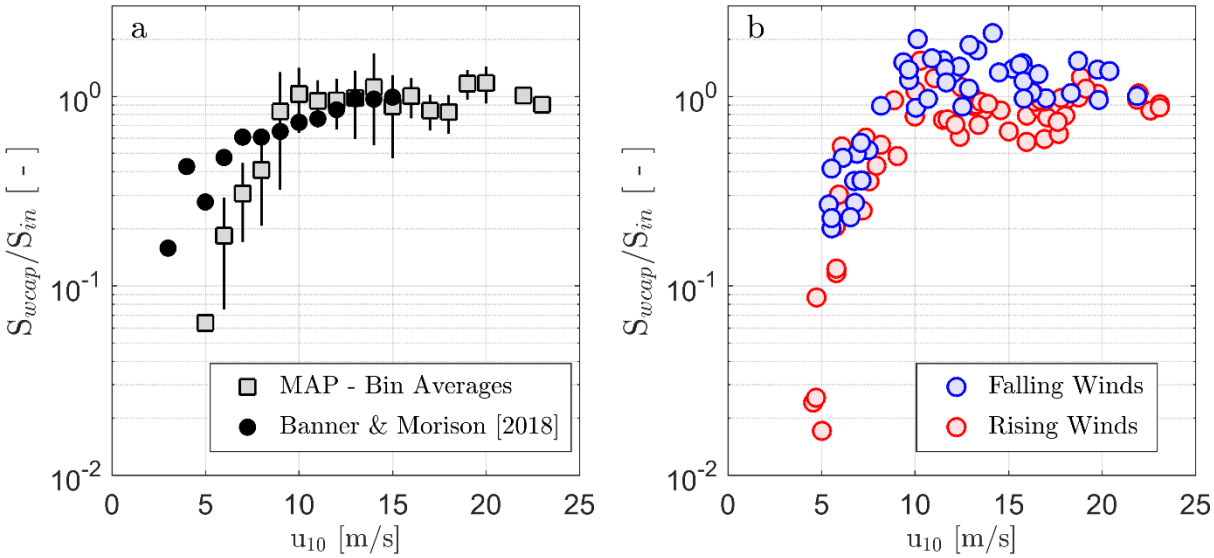

Figure 7(a,b). Panel a shows 1 m/s bin average values of the ratio of energy dissipation rate due to whitecaps, S_{wcap}, to the energy input rate from the wind to the wave field, S_{in}, as a function of wind speed. The S_{wcap} values were estimated using the MAP whitecap coverage dataset from Callaghan et al. (2008) in the context of the energy dissipation based model of whitecap coverage developed in this study. The additional black datapoints are similar estimates taken from figure 13 of Banner and Morison (2018), which were derived from the dataset of Sutherland and Melville (2015). Panel b shows the MAP-derived dataset in panel a, but without bin-averaging. The individual datapoints are classified as either from rising wind conditions (red circles) or falling wind conditions (blue circles), as determined from a wind acceleration analysis detailed in the main text.

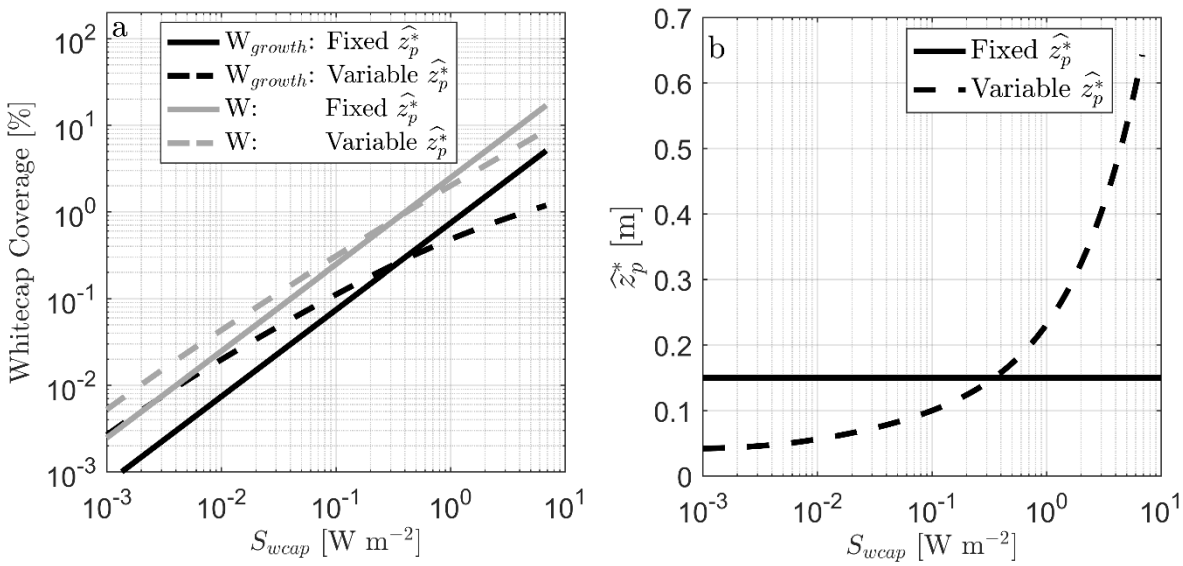

Figure 8(a-b). Panel a shows the variation of W and W_{growth} as a function of S_{wcap} for different values of $\hat{z}_p^*$. The solid lines assume a constant value of 0.15 m. The dashed lines assume a variable $\hat{z}_p^*$ following equation (22). Panel b shows the specific values of $\hat{z}_p^*$ for the S_{wcap} values used.